Hindawi Publishing Corporation
Shock and Vibration
Volume 2015, Article ID 327362, 7 pages
http://dx.doi.org/10.1155/2015/327362

Research Article

Effects of Contraction Joints on Vibrational Characteristics of Arch Dams: Experimental Study

S. S. Wang,[1] Y. F. Zhang,[1] M. S. Cao,[1,2] and W. Xu[1]

[1]*Department of Engineering Mechanics, Hohai University, Nanjing 210098, China*
[2]*Institute of Fluid-Flow Machinery of Polish Academy of Sciences, Ul. Fiszera 14, 80-952 Gdansk, Poland*

Correspondence should be addressed to M. S. Cao; cmszhy@hhu.edu.cn

Received 30 January 2015; Revised 21 July 2015; Accepted 26 July 2015

Academic Editor: M. I. Herreros

Copyright © 2015 S. S. Wang et al. This is an open access article distributed under the Creative Commons Attribution License, which permits unrestricted use, distribution, and reproduction in any medium, provided the original work is properly cited.

This study experimentally investigates the effects of contraction joints on the vibrational characteristics of high arch dams. Three scale models of the world's second highest dam, the Xiaowan Arch Dam, are used as experimental specimens identified by zero, one, and two contraction joints. When a scale model vibrates harmonically at a specific frequency, its operating deflection shape is acquired by using a scanning laser vibrometer to scan the side surface of the model. The effects of contraction joints on the vibrational characteristics of arch dams are studied by examining the changes in operating deflection shapes. Experimental results demonstrate that (i) contraction joints can significantly affect the vibrational characteristics of arch dams, (ii) the operating deflection shape intuitively illustrates the vibrational characteristics of arch dams, and (iii) a scanning laser vibrometer has marked advantages over traditional equipment in accurately and efficiently acquiring full-field dynamic responses of a structure.

1. Introduction

Xiaowan Arch Dam in mainland China is the world's second highest arch dam at 292 m (958 ft) [1–3]. The dynamic properties of the Xiaowan Arch Dam have aroused much attention from researchers around the world [4, 5]. Contraction joints are placed in arch dams to control random cracking that is largely due to reduction in volume or shrinkage as the material hardens [5–10]. Noticeably, the effects of contraction joints on the vibrational characteristics have a key role in the analysis of the dynamic properties of such a high dam. As inherent discontinuities, contraction joints are set up during the dam construction stage [11]. They can alter structural physical properties including stiffness, mass, and damping, hence causing changes in structural dynamic responses such as seismic responses [10].

The effects of contraction joints on the dynamic properties of a dam have been investigated extensively. Representative studies are as follows. Dowling and Hall [5] described a nonlinear finite element procedure for arch dams in which the gradual opening and closing of vertical contraction joints were considered. Ahmadi et al. [6] presented a nonlinear joint element model with coupled shear and tensile effects to model the actions of contraction joints in dam-reservoir systems. Lau et al. [8] modeled a constitutive contraction joint for a zero-thickness joint element in an arch dam model that could simulate both opening and closing and shear sliding behavior, as well as the nonlinear shear key effects of the joint. Azmi and Paultre [10] developed a nonlinear joint element to represent the dynamic behavior of vertical contraction joints in concrete dams, and the element could be used to describe partial joint opening and closing as well as tangential displacement. On the whole, most studies have considered the effects of contraction joints on the seismic response [5–10] using numerical simulations. Noticeably, due to the considerable complexity of the task, few experimental studies are available that inspect the full-field dynamic deformation of a dam.

To remedy this lack of experimental studies, this work experimentally measures the full-field dynamic responses of the Xiaowan Arch Dam to analyze the effects of contraction joints on its dynamic properties. The full-field dynamic response is reflected by an operating deflection shape (ODS). An ODS is an online and in-site dynamic response of a structure that vibrates harmonically due to excitation at a specific

harmonic frequency. Inman [11] elucidated that an ODS was the actual vibrational shape of the displacement or velocity of a structure that vibrates in the steady-state condition in response to a specific structural loading. An ODS of a structure carries dynamic information from a group of mode shapes with their natural frequencies around the structure's vibration frequency [12–14]. An ODS can provide more flexible dynamic information than a mode shape since it can be produced at any single harmonic frequency, not being confined to natural frequencies [15]. The ODS has emerged in a variety of applications pertaining to the analysis of structural dynamic properties, typically structural damage detection [16–18].

Conventional dynamic measurement facilities, for example, acceleration sensors, are inadequate for acquiring the ODS of a scale model of a dam, mainly because it is extremely difficult to deploy a net of acceleration sensors to realize full-field measurement. In particular, the added mass of numerous sensors would alter the dynamic properties of the dam under inspection. However, these deficiencies of conventional facilities can be overcome by a recently developed optical device, the scanning laser vibrometer (SLV) [19]. A SLV primarily features noncontact measurement, high spatial resolution, entirely automatic processing, and high accuracy of measurement [20–23]. With these features, the SLV is suitable for use in measuring the ODS of a dam model.

In this study, a SLV is utilized to acquire the ODS of scale models of the Xiaowan Arch Dam, with the aim of investigating the effects of contraction joints on the vibrational characteristics of arch dams.

2. Definition of ODS

The motion equation for a linear structure with a harmonic excitation acting on the structure is [11]

$$M\ddot{x} + C\dot{x} + Kx = Fe^{j\omega t}, \tag{1}$$

where M, C, and K are the mass, damping, and stiffness matrices, respectively; x, $\dot{x}$, and $\ddot{x}$ are the displacement, velocity, and acceleration, respectively; F is the amplitude of the excitation with the frequency ω.

Under the harmonic excitation $Fe^{j\omega t}$, the displacement response takes the form: $x(t) = ue^{j\omega t}$. Substitution of $x(t) = ue^{j\omega t}$ into (1) yields

$$\left(K - \omega^2 M + j\omega C\right) u = F. \tag{2}$$

Solving (2) yields

$$u = \left(K - \omega^2 M + j\omega C\right)^{-1} F, \tag{3}$$

where $a(\omega) = (K - \omega^2 M + j\omega C)^{-1}$ is the receptance matrix, with which the real part of the steady-state response can be expressed as

$$x(t) = \mathrm{Re}\left(\alpha(\omega) Fe^{j\omega t}\right). \tag{4}$$

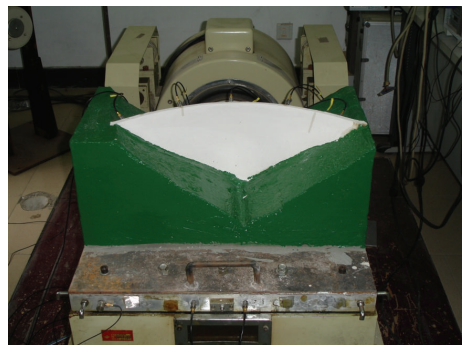

Figure 1: Arch dam model with base-excitation system.

From (4), the real part of the velocity response can be derived as

$$v(t) = \mathrm{Re}\left(j\omega\alpha(\omega) Fe^{j\omega t}\right). \tag{5}$$

The ODS is defined by evaluating (5) at different angles or times for a steady-state harmonic response, with the angle defined by

$$\theta_a = \omega t_a. \tag{6}$$

The ODS can be evaluated at specified angles, $\theta_a = 2\pi a/b$, where b is the number of points in one vibration cycle used to evaluate the ODS and $a = 0, 1, 2, \ldots, b-1$. Therefore, the number of times used to evaluate the ODS is given by

$$t_a(\omega) = \frac{2\pi a}{b\omega}. \tag{7}$$

The velocity ODS is defined by

$$v\left(\frac{\theta_a}{\omega}\right) = \mathrm{Re}\left(j\omega\alpha(\omega) Fe^{j\theta_a}\right), \tag{8}$$

which can be experimentally measured using a SLV [19].

3. Experimental Setup

The Xiaowan Arch Dam [24] serves as the prototype to obtain the experimental specimens for studying the effects of contraction joints on the vibrational characteristics of arch dams. The specimens are three 1/1500-scale unit models (Figure 1) of the full-scale Xiaowan Arch Dam. The principal dimensions of each model are 600 mm, 300 mm, and 250 mm in the length, width, and height directions, respectively. The model is cast using mixed gypsum, barite powder, and water with the compounding ratio of 1 : 1 : 0.78. Each model is identified by the feature of contraction joints: Model I, no contraction joints (Figure 2(a)); Model II, one contraction joint (Figure 2(b)); and Model III, two contraction joints (Figure 2(c)). Each contraction joint is vertical and spans 1 mm in the length direction.

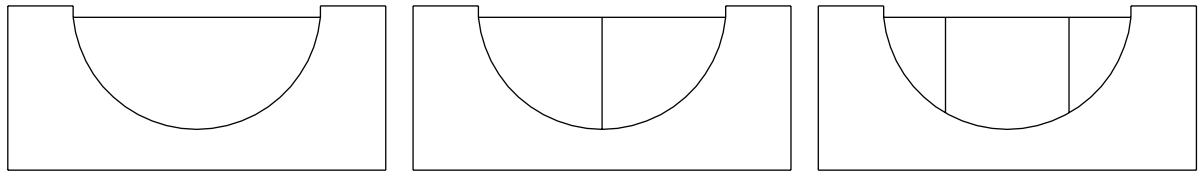

(a) (b) (c)

Figure 2: Scale models identified by number of contraction joints. Model I (a), Model II (b), and Model III (c).

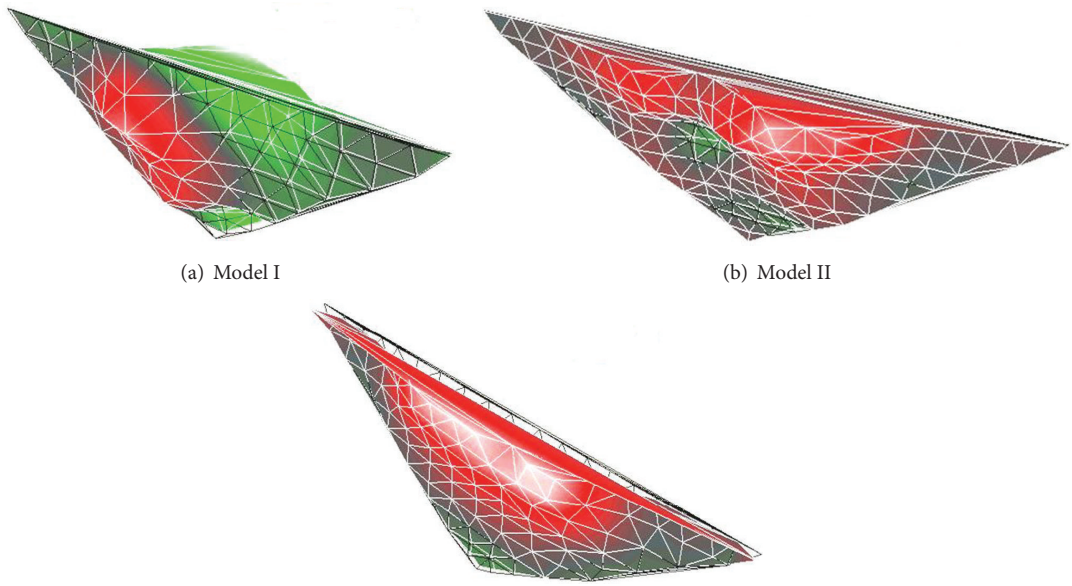

(a) Model I (b) Model II

(c) Model III

Figure 3: First-order mode shape in contrast to initial static shape (plain mesh).

An electromagnetic base-excitation system controlled by a COMET USB shaker control system (Figure 1) is used to harmonically excite the model. As the model vibrates steadily the side surface of the model is scanned by a SLV (Polytec PSV-400) to generate the ODS. The base excitation is fixed at a constant amplitude of acceleration, 5 m/s^2, to align the ODSs of the three models at a comparable level.

4. Results and Discussion

4.1. Natural Frequency and ODS

4.1.1. Natural Frequency. A periodic chirp of increasing frequencies is utilized to excite an arch dam model to generate a dynamic response. The ratio of the response to the chirp in the frequency domain defines a frequency response function (FRF). The peaks of the FRF specify the natural frequencies of the model. From the acquired FRFs, the first natural frequencies, f_1, of three models are identified (Table 1). Clearly, the natural frequency decreases with the increase in the number of the contraction joints. This decrease can be interpreted as the result of the reduction of model stiffness caused by the contraction joints.

Table 1: First natural frequencies (Hz).

Model	I	II	III
f_1	1186.6	874.1	688.4

4.1.2. ODS

(1) Mode Shape. Mode shape dominates an ODS only when the vibration frequency is equal to one of the natural frequencies, in which case a mode shape can be viewed as a particular ODS [18]. A base excitation at f_1 is imposed on the arch dam model. When the model vibrates steadily, the lateral surface of the model is scanned by a SLV to generate the ODS dominated by the corresponding mode shape. The mode shapes obtained are displayed in Figures 3(a), 3(b), and 3(c) for Modes I, II, and III, respectively. In the figures, the velocity nephogram represents the mode shape and the plain mesh designates the initial static shape of the model. The initial static shape acts as a reference to reflect the vibrational deformation carried by the ODS. In Figure 3(c), it can be observed that the base excitation results in a mode shape that deviates from the initial static shape. The ODSs intuitively illustrate

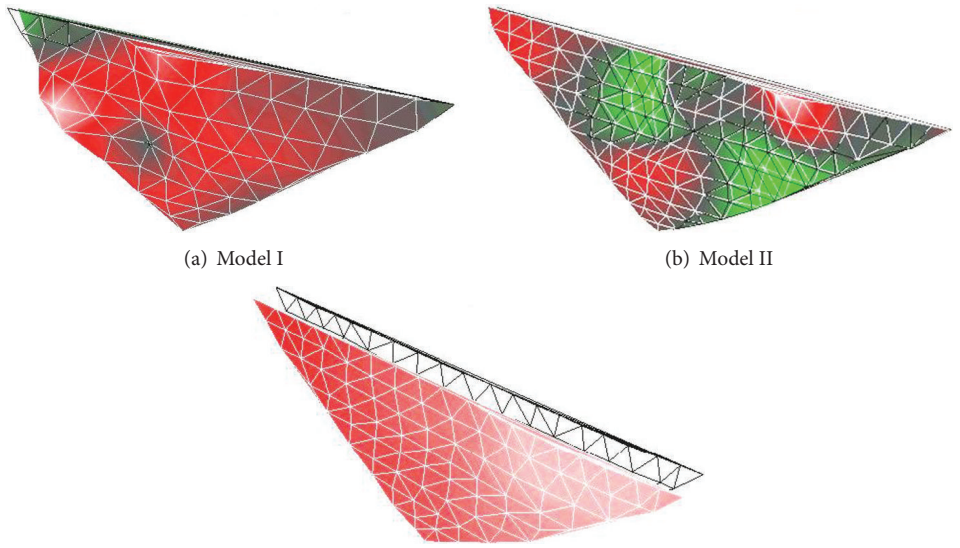

(a) Model I (b) Model II

(c) Model III

Figure 4: ODSs at base excitation of 100 Hz in contrast to initial static shape (plain mesh).

Table 2: Velocity amplitudes at H_1–H_9 for base excitation of 100 Hz (mm/s).

Measurement point	H_1	H_2	H_3	H_4	H_5	H_6	H_7	H_8	H_9
Model I	0.12	0.09	0.04	0.22	0.46	0.20	0.05	0.03	0.02
Model II	0.42	0.17	0.16	0.32	0.11	0.04	0.55	0.11	0.13
Model III	12.19	11.65	12.38	13.68	14.40	16.79	17.80	19.08	16.65

the vibrational characteristics of the models; the discrepancies among the ODSs indicate the effect of contraction joints on the dynamic properties of the models. Since the geometry of the dam is complex, it is not easy to determine a general rule for how the contraction joints affect the ODSs.

(2) ODS for Base Excitation of 100 Hz. An ODS represents a generalized dynamic deflection of a structure under harmonic excitation, possibly caused by active, ambient, or self-excitation [15]. With loss of generality, a much lower frequency of 100 Hz is arbitrarily selected to generate base excitation, giving rise to the ODSs shown in Figures 4(a), 4(b), and 4(c) for Models I, II, and III, respectively. In Figure 4(c), the overall mode shape deviates from the initial static shape as the consequence of the base excitation. In these figures, the ODSs clearly illustrate the vibration of the dam, from which the significant effects of the contraction joints on the vibration deformation are reflected by the changes of the ODSs.

4.2. Pointwise Vibrational Characteristics. To further investigate the effect of contraction joints on the vibrational characteristics of the arch dam model, the pointwise vibration characteristics are analyzed. The pointwise vibration characteristics are assessed using the *velocity amplitude* of vibration at a specified measurement point. Here, *velocity amplitude* means the average of the amplitude of velocity at a point when this point vibrates for sufficient time to accommodate the uncertainty of the vibration. Two groups of measurement points (Figure 5) are considered: one group covers the measurement points from H_1 through H_9 located evenly and horizontally across the top of the model; the other group covers the measurement points from V_1 through V_7 located vertically along the midline of the model.

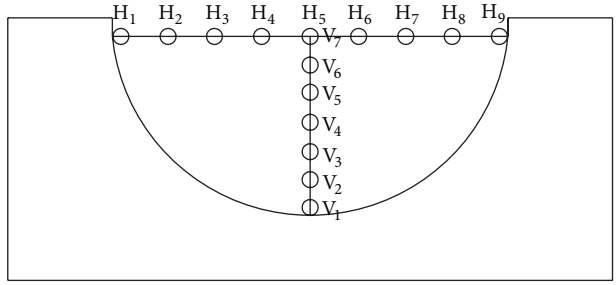

Figure 5: Layout of measurement points.

While a model vibrates steadily due to the base excitation of 100 Hz, the velocity of a specific measurement point is measured by a SLV to obtain a temporal profile, from which the velocity amplitude is evaluated. Table 2 lists the velocity amplitudes at measurement points H_1–H_9 for Models I, II, and III. Comparison of the velocity amplitudes at H_1–H_9 for Models I, II, and III is depicted in Figure 6. Similarly, Table 3 and Figure 7 represent the velocity amplitudes when the model vibrates due to the base excitation of f_1.

Table 3: Velocity amplitudes at H_1–H_9 for base excitation at f_1 (mm/s).

Measurement point	H_1	H_2	H_3	H_4	H_5	H_6	H_7	H_8	H_9
Model I	0.69	1.69	2.42	8.61	17.66	14.10	4.87	1.37	1.21
Model II	0.36	6.14	12.61	6.36	10.88	20.11	21.92	2.67	1.89
Model III	3.51	1.69	3.89	8.87	9.28	9.10	4.33	0.47	2.10

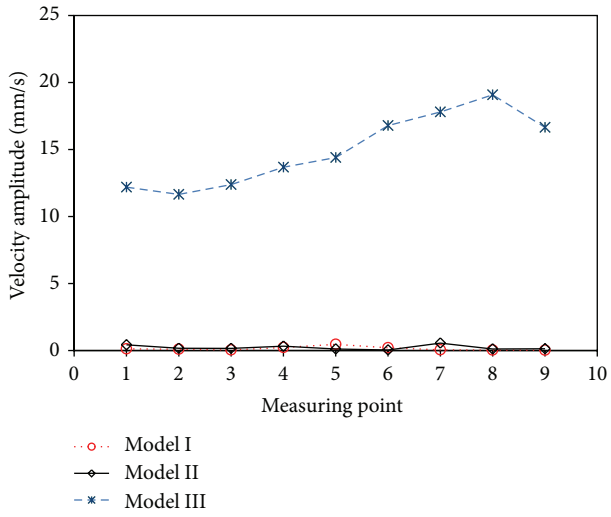

Figure 6: Velocity amplitudes at H_1–H_9 for Models I, II, and III subjected to base excitation at 100 Hz.

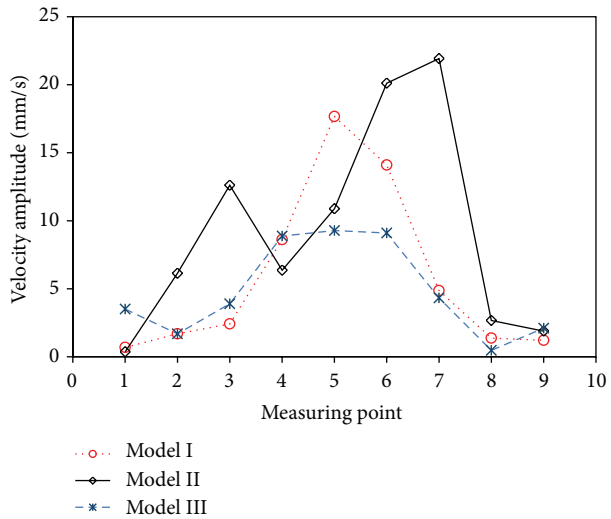

Figure 7: Velocity amplitudes at H_1–H_9 for Models I, II, and III subjected to base excitation at f_1.

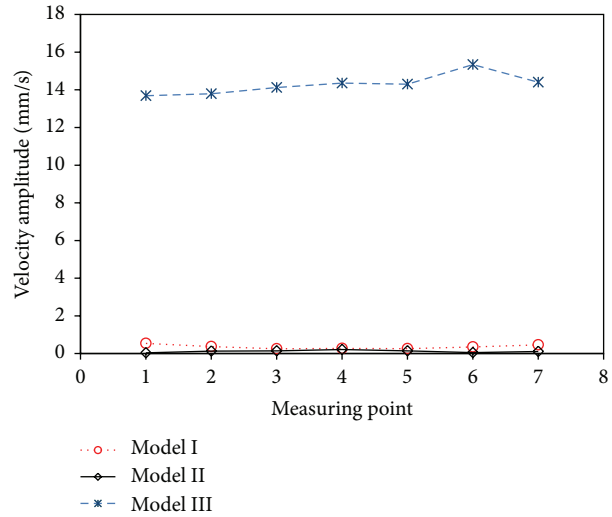

Figure 8: Velocity intensities of V_1–V_7 for Models I, II, and III subjected to base excitation at 100 Hz.

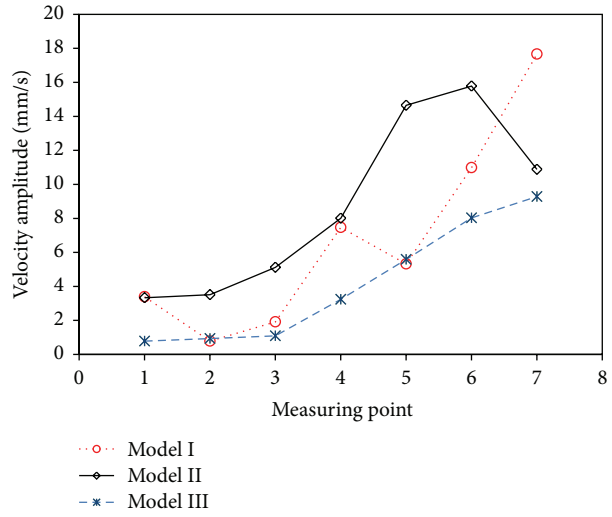

Figure 9: Velocity intensities of V_1–V_7 for Models I, II, and III subjected to base excitation at f_1.

As can be observed from Table 2 and Figure 6, the horizontal velocity amplitude of Model I is similar to that of Model II when each model is subjected to base excitation at 100 Hz, whereas Model III has higher velocity amplitude. In the case of base excitation at f_1, the velocity amplitudes for the three models are at the same level but contain observable differences.

Table 4 presents the vertical velocity amplitudes of V_1–V_7 for Models I, II, and III subjected to base excitation at 100 Hz. Figure 8 displays the vertical comparison of velocity amplitudes for these three models.

The velocity amplitudes of measurement points in the vertical direction subjected to base excitation at f_1 are shown in Table 5. A comparison of the velocity amplitudes for these three models is displayed in Figure 9.

Table 4: Velocity amplitudes at V_1–V_7 for excitation at 100 Hz (mm/s).

Measurement point	V_1	V_2	V_3	V_4	V_5	V_6	V_7
Model I	0.54	0.37	0.25	0.27	0.26	0.35	0.46
Model II	0.04	0.13	0.14	0.21	0.14	0.05	0.11
Model III	13.69	13.79	14.12	14.36	14.30	15.34	14.40

Table 5: Velocity amplitudes at V_1–V_9 for base excitation at f_1 (mm/s).

Measurement point	V_1	V_2	V_3	V_4	V_5	V_6	V_7
Model I	3.39	0.78	1.91	7.47	5.32	10.98	17.66
Model II	3.33	3.51	5.12	8.01	14.65	15.78	10.88
Model III	0.78	0.93	1.09	3.24	5.59	8.03	9.28

Table 4 and Figure 8 show that the velocity amplitudes in the vertical direction are similar for Model I and Model II when each model is subjected to base excitation at 100 Hz, whereas those for Model III are clearly higher. Table 5 and Figure 9 show the velocity amplitudes corresponding to base excitation at f_1, where the lowest velocity amplitude occurs in Model III. Moreover, the structural maximal velocity responses increase from the lower to the upper parts of the model on the whole for all models subjected to base excitation at f_1.

5. Conclusion

Three scale models identified by the feature of contraction joints are elaborated to study the full-field dynamic responses of the well-known Xiaowan Arch Dam. The full-field dynamic response is manifested by the ODS that is measured by a SLV-based optical measurement system. From the ODSs, the effects of contraction joints on the vibrational characteristics of the high arch dam are investigated. Some observations from this expedient study are as follows:

(i) Contraction joints can significantly affect the dynamic property of the arch dam; therefore, their optimal deployment is critical for the performance of the dam.

(ii) The SLV is an advanced tool for acquiring the full-field vibrational deformation of a dam of large volume. This tool is superior to conventional dynamic measurement facilities.

(iii) The results of this study provide a guide for experimental analysis of the dynamic behavior of high arch dams.

Conflict of Interests

The authors declare that there is no conflict of interests regarding the publication of this paper.

Acknowledgments

S. S. Wang acknowledges the financial support of the National Natural Science Foundation of China (Grant nos. 11132003 and 51179064) and the Jiangsu Province's Qing Lan Project of Scientific and Technological Innovation (Grant no. 2014011).

References

[1] J. Chai, Y. Wu, and S. Li, "Analysis of coupled seepage and stress fields in rock mass around the Xiaowan arch dam," *Communications in Numerical Methods in Engineering*, vol. 20, no. 8, pp. 607–617, 2004.

[2] G. Zhang, Y. Liu, and Q. Zhou, "Study on real working performance and overload safety factor of high arch dam," *Science in China Series E: Technological Sciences*, vol. 51, no. 2, pp. 48–59, 2008.

[3] P. Lin, W. Zhou, and H. Liu, "Experimental study on cracking, reinforcement, and overall stability of the Xiaowan super-high arch dam," *Rock Mechanics and Rock Engineering*, vol. 48, no. 2, pp. 819–841, 2014.

[4] X. Du and J. Tu, "Nonlinear seismic response analysis of arch dam-foundation systems—part II opening and closing contact joints," *Bulletin of Earthquake Engineering*, vol. 5, no. 1, pp. 121–133, 2007.

[5] M. J. Dowling and J. F. Hall, "Nonlinear seismic analysis of arch dams," *Journal of Engineering Mechanics*, vol. 115, no. 4, pp. 768–789, 1989.

[6] M. T. Ahmadi, M. Izadinia, and H. Bachmann, "A discrete crack joint model for nonlinear dynamic analysis of concrete arch dam," *Computers and Structures*, vol. 79, no. 4, pp. 403–420, 2001.

[7] G. L. Fenves, S. Mojtahedi, and R. B. Relmer, "Effect of contraction joints on earthquake response of an arch dam," *Journal of Structural Engineering*, vol. 118, no. 4, pp. 1039–1055, 1992.

[8] D. T. Lau, B. Noruziaan, and A. G. Razaqpur, "Modelling of contraction joint and shear sliding effects on earthquake response of arch dams," *Earthquake Engineering and Structural Dynamics*, vol. 27, no. 10, pp. 1013–1029, 1998.

[9] C. Zhang, Y. Xu, G. Wang, and F. Jin, "Non-linear seismic response of arch dams with contraction joint opening and joint reinforcements," *Earthquake Engineering and Structural Dynamics*, vol. 29, no. 10, pp. 1547–1566, 2000.

[10] M. Azmi and P. Paultre, "Three-dimensional analysis of concrete dams including contraction joint non-linearity," *Engineering Structures*, vol. 24, no. 6, pp. 757–771, 2002.

[11] D. J. Inman, *Engineering Vibration*, Prentice Hall, 4th edition, 2013.

[12] K. Waldron, A. Ghoshal, M. J. Schulz et al., "Damage detection using finite element and laser operational deflection shapes," *Finite Elements in Analysis and Design*, vol. 38, no. 3, pp. 193–226, 2002.

[13] G. Teza, A. Galgaro, and F. Moro, "Contactless recognition of concrete surface damage from laser scanning and curvature computation," *NDT & E International*, vol. 42, no. 4, pp. 240–249, 2009.

[14] K. Waldron, A. Ghoshal, M. J. Schulz et al., "Damage detection using finite element and laser operational deflection shapes," *Finite Elements in Analysis and Design*, vol. 38, no. 3, pp. 193–226, 2002.

[15] A. Katunin and P. Przystałka, "Damage assessment in composite plates using fractional wavelet transform of modal shapes with optimized selection of spatial wavelets," *Engineering Applications of Artificial Intelligence*, vol. 30, pp. 73–85, 2014.

[16] A. Katunin, "Damage identification in composite plates using two-dimensional B-spline wavelets," *Mechanical Systems and Signal Processing*, vol. 25, no. 8, pp. 3153–3167, 2011.

[17] P. F. Pai and L. G. Young, "Damage detection of beams using operational deflection shapes," *International Journal of Solids and Structures*, vol. 38, no. 18, pp. 3161–3192, 2001.

[18] W. Xu, M. Radzieński, W. Ostachowicz, and M. S. Cao, "Damage detection in plates using two-dimensional directional Gaussian wavelets and laser scanned operating deflection shapes," *Structural Health Monitoring*, vol. 12, no. 5-6, pp. 457–468, 2013.

[19] A. B. Stanbridge, M. Martarelli, and D. J. Ewins, "Measuring area vibration mode shapes with a continuous-scan LDV," *Measurement*, vol. 35, no. 2, pp. 181–189, 2004.

[20] D. M. Siringoringo and Y. Fujino, "Experimental study of laser Doppler vibrometer and ambient vibration for vibration-based damage detection," *Engineering Structures*, vol. 28, no. 13, pp. 1803–1815, 2006.

[21] A. Z. Khan, A. B. Stanbridge, and D. J. Ewins, "Detecting damage in vibrating structures with a scanning LDV," *Optics and Lasers in Engineering*, vol. 32, no. 6, pp. 583–592, 2000.

[22] W. Waidelich, "Scanning laser vibrometer," in *Laser in der Technik/Laser in Engineering*, pp. 296–298, Springer, Berlin, Germany, 1994.

[23] A. B. Stanbridge and D. J. Ewins, "Modal testing using a scanning laser Doppler vibrometer," *Mechanical Systems and Signal Processing*, vol. 13, no. 2, pp. 255–270, 1999.

[24] S. S. Wang, Z. H. Zhao, M. S. Cao, X. M. Li, and Y. R. Zhang, "Scale effects on structural dynamic properties and responses: illustrated on arch dams," *Journal of Vibroengineering*, vol. 16, no. 8, pp. 4026–4038, 2014.

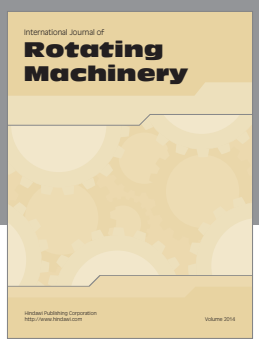

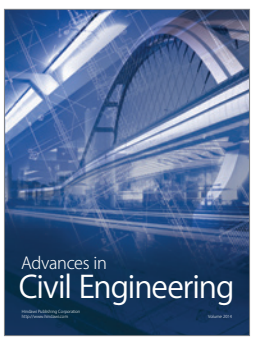

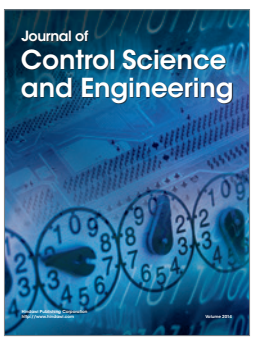

Hindawi
Submit your manuscripts at
http://www.hindawi.com